Semi-continuous propagation of influenza A virus and its defective interfering particles: analyzing the dynamic competition to select candidates for antiviral therapy

Lars Pelz[1, †], Daniel Rüdiger[1, †], Fadi G. Alnaji[2], Yvonne Genzel[1], Christopher B. Brooke[2], Sascha Y. Kupke[1,*], Udo Reichl[1,3]

[1]Max Planck Institute for Dynamics of Complex Technical Systems, Bioprocess Engineering, Magdeburg, Germany

[2]University of Illinois at Urbana-Champaign, Department of Microbiology, Urbana, Illinois, USA

[3]Otto-von-Guericke-University Magdeburg, Chair of Bioprocess Engineering, Magdeburg, Germany

[†]These authors contributed equally to this work.

*** Correspondence:**

Sascha Y. Kupke

kupke@mpi-magdeburg.mpg.de

Keywords: Influenza A virus, defective interfering particles, antiviral, next-generation sequencing, dynamics, two-stage bioreactor

Abstract

Defective interfering particles (DIPs) of influenza A virus (IAV) are naturally occurring mutants that comprise internal deletions in at least one of their eight viral RNA (vRNA) segments. Upon co-infection with infectious standard virus (STV), DIPs interfere with the viral replication cycle rendering them candidates for antiviral therapy. To study the propagation competition between

defective interfering (DI) vRNAs, we used a small-scale two-stage cultivation system for semi-continuous propagation of IAV. Strong periodic oscillations in virus titers were observed due to the dynamic interaction of DIPs and STV. Using next generation sequencing, we found a predominant formation and accumulation of DI vRNAs on the polymerase segments. Short DI vRNAs accumulated stronger than longer ones, indicating a replication advantage. However, a sweet spot of fragment length was observed. Some DI vRNAs, including highly accumulated ones, showed breaking points in a specific part of their bundling signal, suggesting its dispensability for DI vRNA propagation. Over a total cultivation time of 21 days post infection, several distinct DI vRNAs accumulated to high levels, while others decreased. Assuming that DIPs replicating to high copy numbers have a high capacity to interfere with STV replication, we suggest candidates for efficacious antiviral treatment.

1 Introduction

Yearly, on average 400,000 people globally die from an infection with seasonal influenza A virus (IAV) (Paget et al., 2019). Moreover, the potential emergence of pandemic strains is a major threat to the public health. The most effective prevention of influenza is vaccination with tri- or quadrivalent formulations, which provide protection against different influenza virus strains (Moa et al., 2016; Samson et al., 2019). However, influenza vaccines have to be reformulated annually as a result of antigenic drifts (Vogel and Manicassamy, 2020). This is associated with a potential decrease in vaccine efficacy due to false predictions and a mismatch of circulating strains as discussed in a recent review (Tricco et al., 2013). Furthermore, antiviral drugs targeting the viral neuraminidase (oseltamivir, zanamivir) (Paules and Subbarao, 2017) or the viral endonuclease (baloxavir) (O'Hanlon and Shaw, 2019) may also be used. Yet, circulating strains have already shown resistance against available antivirals (Hayden et al., 2018; Hurt et al., 2009; Jones et al.,

2018). Therefore, the development of effective prophylactic and therapeutic treatment options is urgently needed.

One promising approach for antiviral therapy is the application of defective interfering particles (DIPs) (Dimmock and Easton, 2014; Huo et al., 2020; Vignuzzi and Lopez, 2019; Yang et al., 2019; Zhao et al., 2018). These naturally existing viral mutants feature an internal deletion in their viral genome, which renders them defective in virus replication. In addition, a new species of DIPs that showed point mutations on segment (Seg) 7 vRNA was discovered recently (Kupke et al., 2019). DIPs can only replicate in a co-infection with infectious standard virus (STV), which complements the respective defect of the DIPs. These viral mutants are believed to interfere by preferential replication of the defective interfering (DI) vRNA in comparison to the full-length (FL) vRNA (Laske et al., 2016; Marriott and Dimmock, 2010; Nayak et al., 1985). Furthermore, interference was shown for the packaging step, as DI vRNAs selectively outcompeted FL vRNAs (Duhaut and McCauley, 1996; Odagiri and Tashiro, 1997). Notably, in mouse and ferret models, the administration of DIPs showed a pronounced antiviral effect against IAV (Dimmock et al., 2012; Dimmock et al., 2008; Hein et al., 2020; Huo et al., 2020; Zhao et al., 2018).

Packaging of progeny virions of IAV is a complex process. The leading packaging model postulates a selective packaging of the eight different vRNA genome segments (Hutchinson et al., 2010; Noda and Kawaoka, 2010). Decisive for correct and efficient packaging is a special vRNA sequence (packaging signal), which was discovered using reverse genetics approaches (Fujii et al., 2003). As DIPs comprise a truncated segment, this packaging signal might equally be affected. However, it was suggested that this packaging signal in the shortened segment typically remains intact (Dimmock and Easton, 2014; Hutchinson et al., 2010). Moreover, it was proposed that a minimum sequence length within the truncated segment on Seg 1 is required not only for DI vRNA

stability (Duhaut and Dimmock, 2000), but also for interference with FL vRNA (Duhaut and Dimmock, 2002). However, no systematic study was conducted for the other segments, so far, and only limited data about sequence lengths of DI vRNAs on non-polymerase segments is available (Duhaut and Dimmock, 1998; Duhaut and McCauley, 1996; Jennings et al., 1983).

Recently, cell culture-based production in a two-stage bioreactor system was shown for a specific DIP (DI244) (Tapia et al., 2019). In a continuous culture, the co-infection with STV resulted in periodic oscillations of virus titers. Moreover, formation and accumulation of other emerging DI vRNAs was observed. Using a simplified set-up, we established a semi-continuous IAV propagation system to thoroughly investigate the selection of competitive DIPs. More specifically, DIPs are in a competition for cellular and viral resources, but also for packaging and, thus, for propagation. As a result, DIPs that prevail over others are likely more competitive and might have a higher potential for interference with STV. This assumption is based on the fact that the shortage of resources for STV production is a mechanism of DIPs to interfere with virus replication (Marriott and Dimmock, 2010), however, interference with STV was also shown for the packaging step (Duhaut and McCauley, 1996; Odagiri and Tashiro, 1997). For in-depth characterization of the dynamics, we used a recently published next-generation sequencing (NGS) framework that enabled the specific detection and quantification of distinct deletion junctions on the IAV vRNA level (Alnaji et al., 2019). Results showed that DI vRNAs *de novo* formation and accumulation occurred almost exclusively for segments related to the viral polymerase, i.e. Seg 1, 2, and 3. Moreover, a preferential accumulation towards shorter DI vRNAs was observed together with a favorite fragment length (sweet spot) of each segment. Analysis of deletion junction sites of DI vRNAs (including highly accumulated ones) demonstrated that the incorporation signal, but not the entire bundling signal is required for DIP spreading. We identified a small subset of highly

abundant DI vRNAs after a total cultivation period of 21 days post infection (dpi) that could be promising candidates for antiviral therapy.

2 Materials and Methods

2.1 Cells and viruses

An adherent Madin-Darby canine kidney (MDCK) cell line (ECACC, No. 84121903) was adapted in previous works to grow in suspension culture (Lohr et al., 2010) in chemically defined Xeno™ medium (Bissinger et al., 2019), hereafter referred to as MDCKsus. Cultivation of MDCKsus cells was conducted in shake flasks at a working volume of 50 mL (125 mL baffled Erlenmeyer Flask, Thermo Fisher Scientific, 4116-0125) using an orbital shaker (Multitron Pro, Infors HT; 50 mm shaking orbit) at 185 rpm and 37°C in a 5% CO_2 environment. The medium was supplemented with 8 mM glutamine. Cell passaging took place every 2–3 days at a seeding viable cell concentration of 1 or 0.5×10^6 cells/mL, respectively. Quantification of viable cell concentration (VCC), viability and diameter were performed using a cell counter (Vi-Cell™ XR, Beckman coulter, #731050). Adherent MDCK cells, in the following denoted as MDCKadh, were maintained in Glasgow minimum essential medium (GMEM, Thermo Fisher Scientific, #221000093) supplemented with 10% fetal bovine serum and 1% peptone at 37°C and 5% CO_2.

For infection, the IAV strain A/PR/8/34 of the subtype H1N1 (provided by Robert Koch Institute, Berlin, Germany), hereafter referred to as PR8, was used (Bissinger et al., 2019). Adaptation to MDCKsus cells and depletion of DI vRNAs of PR8 was carried out over five passages at very low multiplicity of infection (MOI) 10^{-5} (infectivity determined by $TCID_{50}$ assay (Genzel and Reichl, 2007)).

2.2 Small-scale two-stage cultivation system for semi-continuous STV/DIP propagation

For the semi-continuous propagation of PR8, a two-stage cultivation system was used, which consisted of two baffled shake flasks (250 mL baffled Erlenmeyer Flask, Thermo Fisher Scientific, 4116-0250) connected in series (Fig. 1B). The cell seeding shake flask (CSS) and the virus shake flasks (VS) were operated at a working volume of 90.00 mL and 77.52 mL, respectively. MDCKsus cells in exponential growth phase were seeded at a viable cell concentration (VCC) of 0.6×10^6 cells/mL and were cultivated in batch mode at 185 rpm, and 37°C in a 5% CO_2 environment for 2 days. When VCC reached approximately 3.0×10^6 cells/mL, at -1.6 dpi, a calculated volume of cell suspension was harvested every 12 h, while pre-warmed fresh medium was added manually to obtain a residence time (RT, inverse of the dilution rate) of 38.3 h (both, CSS and VS). Please note that both shake flasks were not yet connected in series. After steady state was achieved, the cells in the VS were infected with PR8 at a MOI of 0.1 and trypsin (Thermo Fisher Scientific, #27250-018) was added (final activity of 20 U/mL). At 12 hpi, semi-continuous production was started by transferring cells from the CSS to the VS (V_2). Furthermore, virus was harvested (V_4) and both shake flasks were filled up with pre-warmed fresh medium (V_1 or V_3) to obtain a RT of 38.3 h and 22.0 h for CSS and VS, respectively. Of importance is that the fresh medium, which was added to the VS, contained 60 U/mL trypsin to reach 20 U/mL in the VS. The respective transferred volumes are indicated (Equation 1–4). The RT of 22.0 h for the VS was chosen as previously published data showed a pronounced DIP/STV replication dynamic (Tapia et al., 2019). In addition, samples were taken from the virus harvest at every volume transfer for analysis of VCC, viability, infectious virus titer ($TCID_{50}$), segment-specific PCR and RT-qPCR, and NGS. Sampling of the CSS comprised only VCC, viability and pH value. Cell-free supernatants (300×g, 4°C, 5 min,) were stored at -80°C for further analysis.

$$V_1 = (t_n - t_{n-1}) \cdot V_{CSS} \cdot D_{CSS} \quad (1)$$

$$V_2 = V_1 = (t_n - t_{n-1}) \cdot V_{CSS} \cdot D_{CSS} \quad (2)$$

$$V_3 = (t_n - t_{n-1}) \cdot (V_{VS} \cdot D_{VS} - V_{CSS} \cdot D_{CSS}) \quad (3)$$

$$V_4 = (t_n - t_{n-1}) \cdot D_{VS} \cdot V_{VS} \quad (4)$$

Where t_n denotes the sample time point, and t_{n-1} the previous sample time point. V_{CSS} is the volume of the CSS, V_{VS} is the volume of VS, D_{CSS} is the dilution rate of CSS, D_{VS} is the dilution rate of VS. V_{CSS}, D_{CSS}, D_{VS} were predefined as mentioned above. V_3 was set as $0.5 \times V_2$ to ensure a sufficient volume of fresh medium in the VS. This assumption was applied to calculate the volume of V_{Vs}.

2.3 TCID$_{50}$ assay

Quantification of infectious virus titer was performed by TCID$_{50}$ assay (Genzel and Reichl, 2007).

2.4 PCR measurements

Genomic vRNA in progeny virions were examined using PCR. In brief, isolation of vRNA from 150 µL cell-free supernatants was carried out with the NucleoSpin RNA virus kit (Macherey-Nagel, 740956) as described in the manufacturers´ instructions. In order to analyze the presence of FL vRNA and DI vRNA (truncated form), segment-specific PCR was performed (see 2.4.1). Real-time reverse transcription qPCR (real-time RT-qPCR) was applied for absolute quantification of Seg 5 vRNA in the progeny virions (see 2.4.2).

2.4.1 Segment-specific PCR

A recently described method was utilized for segment-specific PCR (Frensing et al., 2013; Kupke et al., 2019). In brief, isolated vRNA was reverse transcribed into cDNA using universal primers that bind at conserved terminal regions of all eight IAV genome segments (Supplementary Table 1). Subsequently, segment-specific primers were used for amplification of the respective genome segment by PCR (Supplementary Table 1). Finally, PCR products were analyzed by gel electrophoresis.

2.4.2 Real-time RT-qPCR

A recently reported method for the specific detection and quantification of influenza viral RNA segments using real-time RT-qPCR was employed (Frensing et al., 2016; Kawakami et al., 2011; Kupke et al., 2019). For this, RNA reference standards were *in vitro* synthesized for absolute quantification (Supplementary Table 4). Isolated vRNA of the samples was used for reverse transcription (Supplementary Table 2), followed by real-time qPCR (based on SYBR green detection) (Supplementary Table 3). Calculation for absolute quantification of vRNA of Seg 5 was conducted as previously described (Frensing et al., 2016; Kupke et al., 2019)

2.4.3 NGS and data processing

Sample preparation, NGS library preparation and sequencing analysis of deletion junctions was performed according to a recently published study (Alnaji et al., 2019)

2.5 Analysis of deletion junctions

Deletion junctions refer to the DI vRNAs in the viral population, while deletion junction sites refer to the start and end position of the breaking point in the viral genome. Deletion junctions that did not accumulate to levels above 14 NGS reads in at least one sampling time point were removed

from the data set for higher accuracy (Alnaji et al., 2019). Furthermore, defective vRNAs that showed still more than 85 % vRNA of the FL segment were excluded from analysis in this work (except for Supplementary Fig. 2B). DI vRNA 3´ and 5’ length indicated the number of retained nucleotides prior and after the deletion junction at the respective vRNA end. Of note is that DI vRNA was reported as negative-sense, in 3´ to 5´ orientation. The reference genome used for alignment and calculation of the DI vRNA length comprised the following sequence lengths: Seg 1 (2341 nucleotides (nt)), Seg 2 (2341 nt), Seg 3 (2233 nt), Seg 4 (1775 nt), Seg 5 (1565 nt), Seg 6 (1413 nt), Seg 7 (1027 nt), Seg 8 (890 nt). Number of nucleotides of the incorporation signal (non-coding region (NCR)) and the bundling signal (terminal ends of coding region), which together form the packaging signal, were taken from a recent review (Breen et al., 2016).

3 Results

3.1 Semi-continuous production of IAV results in periodic oscillations of virus titers and strong accumulation of DIPs

In order to induce *de novo* generation and accumulation of DIPs, PR8 was propagated in a semi-continuous small-scale two-stage cultivation system (Fig. 1B). For infection, we used a seed virus that was depleted in DI vRNAs as shown by segment-specific RT-PCR (Fig. 1A). MDCKsus cells were seeded into the CSS and VS at a VCC of 0.6×10^6 cells/mL and grown in batch mode to about 3.0×10^6 cells/mL (-1.6 dpi) (Supplementary Fig. 1). Subsequently, for both shake flasks, a calculated volume of cell suspension was discarded and fresh medium was added at regular time intervals (both shake flasks not yet connected in series). This resulted in a RT of 38.3 h for both vessels. Note that preliminary studies showed a steady state in the VCC for this RT (data not shown). Once the steady state was reached (Supplementary Fig. 1), cells in the VS were infected

with PR8 at a MOI of 0.1. At 0.5 dpi, both vessels were connected in series and, from thereon, cells transferred semi-continuously from the CSS to the VS (V_2). In addition, fresh medium was added to both shake flasks (V_1 or V_3) and virus harvest was taken (V_4). The RT was chosen 38.3 h and 22.0 h for CSS and VS, respectively, as this previously resulted in pronounced titer fluctuations and strong accumulation of DIPs (Tapia et al., 2019).

Over the production time of 21 dpi, the steady state in the CSS was kept with an average VCC of 2.6×10^6 cells/mL (SD of $\pm 0.2 \times 10^6$ cells/mL) (Supplementary Fig. 1). As expected, strong periodic oscillations in the infectious virus titers (quantified by $TCID_{50}$ assay) and in the extracellular vRNA level of Seg 5 (quantified by real-time RT-qPCR) were observed in the VS (Fig. 1C). The extracellular vRNA level of Seg 5 was taken as a measure of the total virus number as it is assumed to be highly correlated with the total virus particle concentration. DI vRNAs are mostly found on polymerase segments (Davis and Nayak, 1979; Duhaut and Dimmock, 1998; Jennings et al., 1983; Nayak et al., 1985; Saira et al., 2013), so the occurrence of DIPs should not affect the level of Seg 5 vRNA. Furthermore, STVs and DIPs both incorporate FL Seg 5 vRNA. Shortly after infection at 0.5 dpi, a maximum infectious virus titer of 5.6×10^8 $TCID_{50}$/mL was reached. Here, high concentrations of STV (complying with a high MOI) increased the chance for co-infections with DIPs. Thus, a strong DIP propagation likely occurred early in cultivation, impeding STV propagation. Therefore, infectious virus titers decreased from 0.5 dpi onwards. Eventually, the declining infectious virus titers led to fewer co-infections. Thus, DIP replication decreased, and the total virus particle concentration dropped as well. Additionally, DIPs were out-diluted because of the semi-continuous feeding strategy. Then, at a low infectious virus concentration (complying with a low MOI condition, ~4.0 dpi), the chance of DIP co-infections was significantly reduced. In these conditions, STVs could accumulate again to high virus titers

towards 5 dpi. In the following, further periodic oscillations in virus titers occurred based on the described DIP/STV interaction.

The dynamics in virus titers was well in agreement with results of the segment-specific RT-PCR, for FL and DI vRNAs (Fig. 1D). A rapid accumulation of DI vRNAs occurred already at 0.5 dpi. Furthermore, the FL vRNA signal gradually dropped between 1 dpi and 2.5 dpi, suggesting the preferential production of DI vRNAs. Subsequently, DI vRNA replication decreased and DI vRNAs were washed out, as indicated by weaker band intensities of DI vRNAs (e.g. at 8.5 dpi). Next, correlated with the increase of infectious viral titers (STVs), FL vRNA bands were visible again (e.g. at 9 dpi). Moreover, agarose gels indicated the presence of DI vRNA bands at the end of cultivation that may have been already present in the seed virus, suggesting that some DI vRNAs were preserved. In addition, weak DI vRNA bands as well as undefined, blurred bands emerged during the course of IAV replication, suggesting the formation and accumulation of *de novo* generated DI vRNAs.

In summary, the semi-continuous production of IAV using a seed virus depleted in DI vRNAs led to the expected accumulation of DIPs. Thus, strong periodic oscillations in the total concentration of virions and infectious virus titers were observed due to the dynamic interaction of STVs and DIPs. Moreover, in the course of production, DIPs were exposed to high and low MOI conditions that may have resulted in diverse selection pressures for potential selection of very fit DIPs.

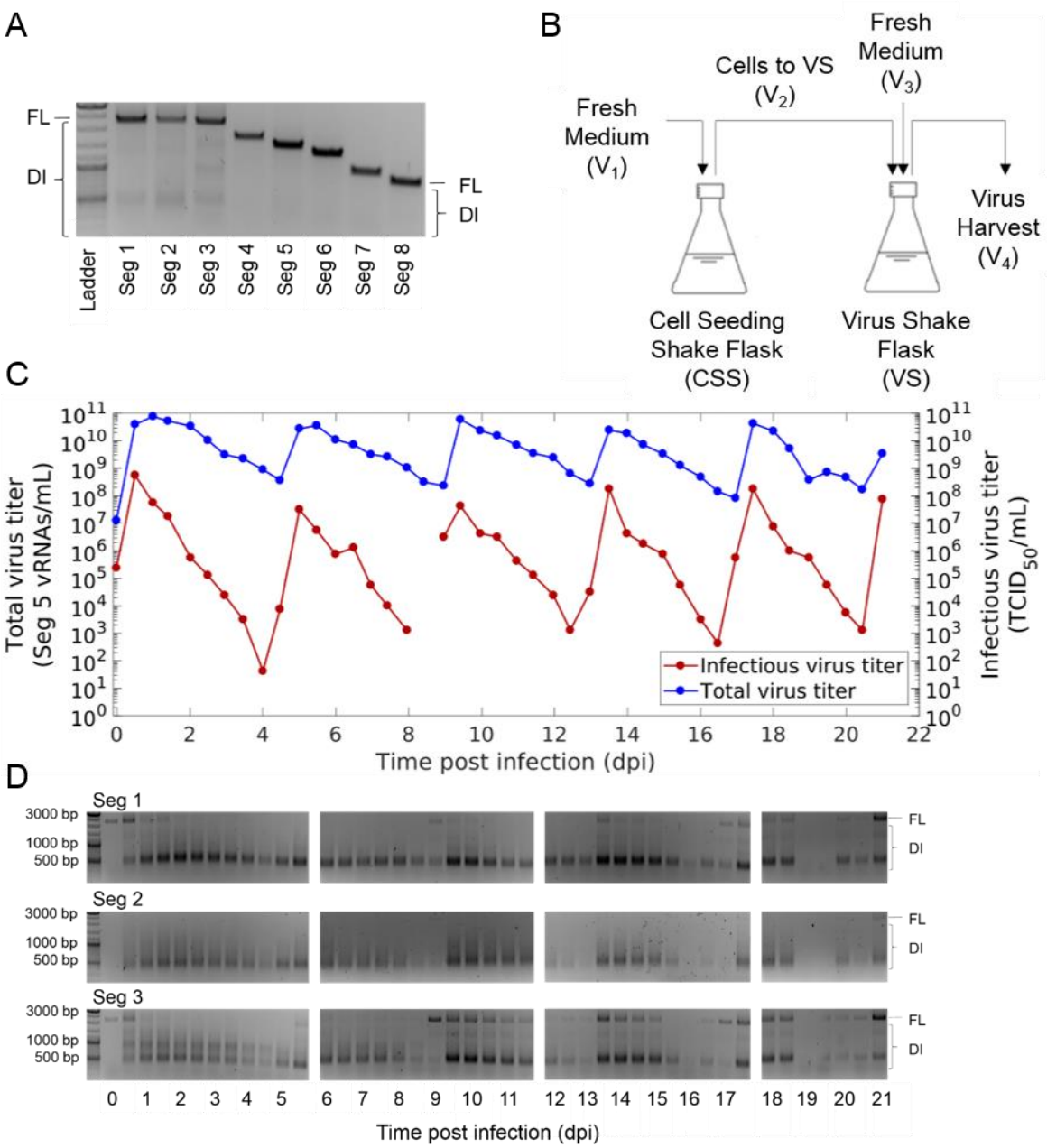

Figure 1: Semi-continuous production of influenza A virus. (A) PR8 seed virus depleted in DI vRNAs used for infection. Results of segment-specific RT-PCR for Seg 1 to 8 followed by agarose gel electrophoresis are shown. Signals corresponding to FL and DI vRNAs are indicated. Upper, middle and lower bands of the DNA ladder indicate 3000, 1000 and 500 bp, respectively. (B) Experimental setup of the small-scale two-stage cultivation system in shake flasks (scheme adapted from Tapia et al. (2017)). MDCKsus cells were grown in the CSS and VS. After an initial batch and semi-continuous phase (CSS and VS not coupled), the cells in the VS were infected with the seed virus (A) at a MOI of 0.1. The semi-continuous production mode was initiated 0.5 dpi, where cells were transferred from the CSS into the VS (V_2) at regular time intervals, while fresh medium was added (V_1 or V_3) and virus harvest was taken for monitoring (V_4). (C) Periodic oscillations of total and infectious virus titers during the production. vRNA level of Seg 5 (indicating total virus particle concentration) was quantified by real-time RT-qPCR and infectious virus titer by

$TCID_{50}$ assay. D) Accumulation of DI vRNAs over the semi-continuous production. Results of the segment-specific RT-PCR are shown for Seg 1, 2, and 3. Signals corresponding to FL and DI vRNAs are indicated. Illustration includes results of one experiment and single measurements.

3.2 Next-generation sequencing indicates the predominant *de novo* formation and accumulation of deletion junctions on polymerase segments

Segment-specific RT-PCR does not enable the specific detection and quantification of distinct deletion junctions. Therefore, to study the diversity of DI vRNAs generated during semi-continuous IAV propagation, samples were subjected to Illumina-based NGS and processed by a bioinformatics pipeline (Alnaji et al., 2019). In brief, vRNA from the produced progeny virions were sequenced by NGS. Reads comprising a deletion junction (DI vRNA reads) do not align to the corresponding reference genome. Thus, these NGS reads were processed by the ViReMa algorithm to identify the position of distinct deletion junctions (Routh and Johnson, 2014).

It has been reported that deletion junctions are mainly found on Seg 1–3 (Davis and Nayak, 1979; Duhaut and Dimmock, 1998; Frensing et al., 2013; Nayak et al., 1985; Saira et al., 2013). To confirm this observation, we investigated the diversity and distribution of deletion junctions on the different vRNA segments in our cultivation system (Fig. 2A and Fig. 2B, respectively). As expected, the highest variation was found on the polymerase segments 1–3, which encode for the polymerase basic protein 2 (PB2) and 1 (PB1), and polymerase acidic protein (PA), respectively (Fig. 2A). The highest number of distinct deletion junctions, i.e. 709, was found for Seg 2 at 5 dpi. Fig. 2B shows the fraction of deletion junctions of each genome segment over time. This fraction describes the ratio of the total number of detected deletion junctions for one segment compared to the total number of deletion junctions on all genome segments. Overall, the fractions of deletion

junctions on polymerase segments were relatively stable over the course of cultivation with the Seg 2 (PB1) fraction mostly exceeding that of Seg 3 (PA) and 1 (PB2) (Fig. 2B). In contrast, deletion junctions of non-polymerase segments showed a significantly lower fraction, which increased slightly towards the end of cultivation but always remained below 2%. As non-polymerase segment deletion junctions occurred only in negligible numbers, they were not considered any further in subsequent analyses.

Next, we investigated the *de novo* formation of DI vRNAs over the course of the cultivation. Fig. 2C shows, at specific time points, the number of *de novo* generated deletion junctions not detected in the seed virus. As indicated before, *de novo* formation occurred mainly on the polymerase segments. In comparison, only a negligible number of *de novo* DI vRNAs was found on the non-polymerase segments (data not shown). Interestingly, most *de novo* formations occurred within the first 1.5 dpi. In addition, a considerable number of *de novo* DI vRNAs was detected between 3.5–5.5 dpi. However, *de novo* formation was significantly lower at later time points. Moreover, the increase in the number of new deletions was highly correlated with an increase in the total virus particle concentration (indicated by the vRNA level of Seg 5) (Fig. 2C). This is consistent with a fast STV replication, and thus, likely with a higher occurrence of the *de novo* formation of DI vRNAs due to the error-prone nature in the replication of the IAV RNA-dependent RNA polymerase.

In sum, our results show that DI vRNAs are predominantly *de novo* formed and accumulated on the polymerase segments during semi-continuous cultivations.

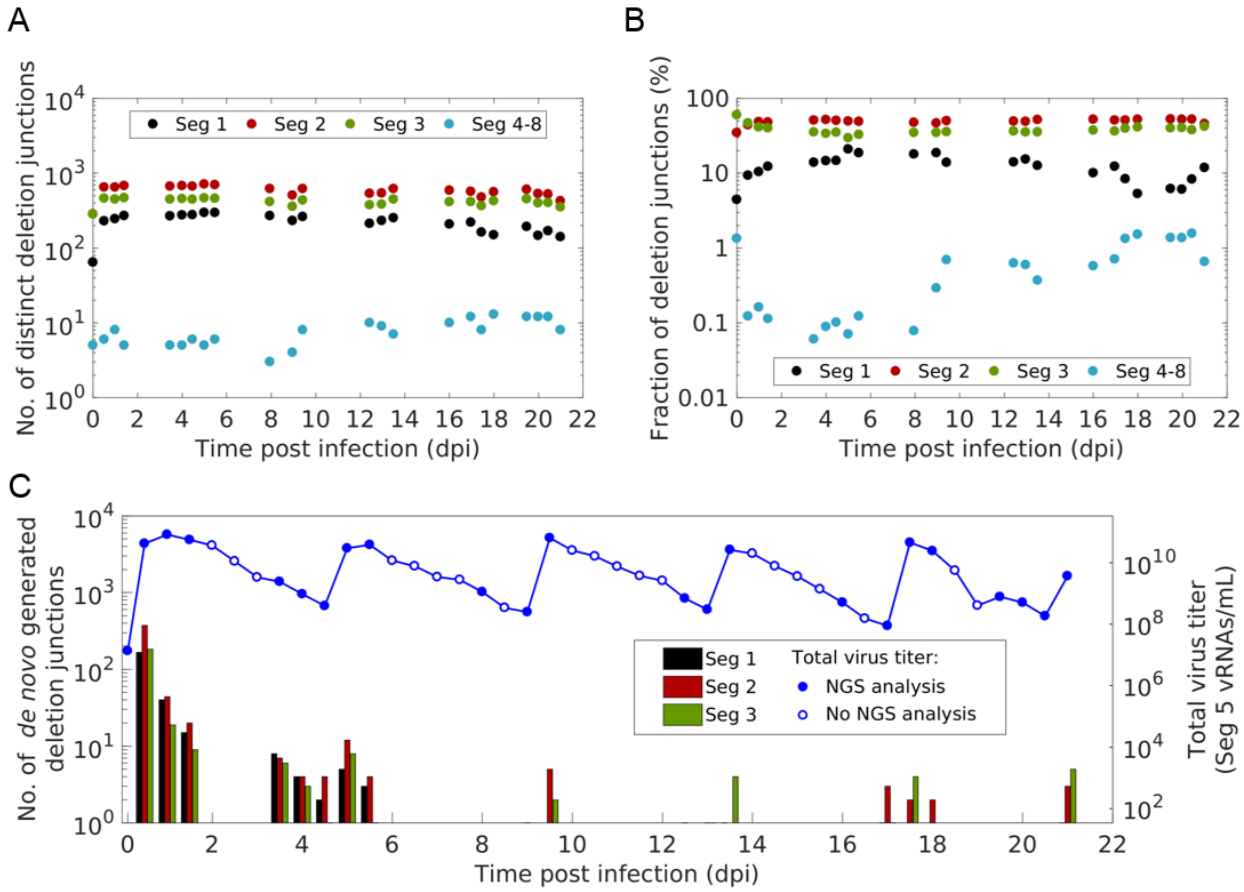

Figure 2: Diversity, distribution and *de novo* generation of deletion junctions during semi-continuous propagation of IAV. Deletion junctions were identified by Illumina-based NGS and subsequent analysis via the ViReMa algorithm (Alnaji et al., 2019). (A) Number of distinct deletion junctions on the respective genome segment(s). (B) Fraction of deletion junctions on the respective genome segment(s). This fraction describes the ratio of the total number of detected deletion junctions for one segment compared to the total number of deletion junctions on all genome segments**.** (C) *De novo* formation of deletion junctions. vRNA level of Seg 5 (indicating total virus particle concentration, as shown in Fig. 1C) was quantified by real-time RT-qPCR. Samples not analyzed by NGS are indicated by blank dots. Illustration includes results of one experiment and a single measurement.

3.3 Short DI vRNAs tend to accumulate to higher levels than longer ones; yet, intermediate length sweet spots were observed

It was reported that DI vRNAs accumulation surpasses that of FL vRNAs due to their shorter length resulting in a supposedly faster replication (Dimmock and Easton, 2014; Nayak et al., 1985).

Therefore, we speculated that shorter DI vRNAs may also accumulate to higher abundances than longer DI vRNAs. Fig. 3 shows the fraction of distinct deletion junctions and their corresponding DI vRNA length. Indeed, a bias towards shorter DI vRNAs was observed that accumulated to higher fractions than longer ones during semi-continuous production (Fig. 3). However, highest abundances were not found for the shortest DI vRNAs. It rather appeared that highest fractions were found at a length sweet spot. To visualize this sweet spot during the semi-continuous production run, we fitted a normal distribution function to the DI vRNA length (Supplementary Fig. 2A), and plotted the resulting mean as a dashed vertical line (Fig. 3). Over the whole cultivation, the mean DI vRNA length ranged between 366–414 nt, 425–534 nt, and 434–557 nt for Seg 1, 2, and 3, respectively.

Moreover, a few larger DI vRNAs (comprising a sequence length of up to 1000 nt) accumulated to high fractions, suggesting that the sequence and the position of the deletion junction may be another factor to consider for replication of a DIP (Fig. 3). Note that Fig. 3 only shows DI vRNAs up to 1000 nt in length, although we also detected very long DI vRNAs (>2000 nt) (Supplementary Fig. 2B). These DI vRNAs with very short deletions may either not result in a defective vRNA, comprise two deletions or represent technical artifacts. Due to their unknown origin and function, defective vRNAs larger than 85 % of its respective FL length were excluded from analysis in this work (except for Supplementary Fig. 2B).

Taken together, shorter DI vRNAs showed a stronger overall accumulation compared to longer DI vRNAs. However, highest abundances were found at a sweet spot, indicative for an optimal length for DI vRNA replication and spreading.

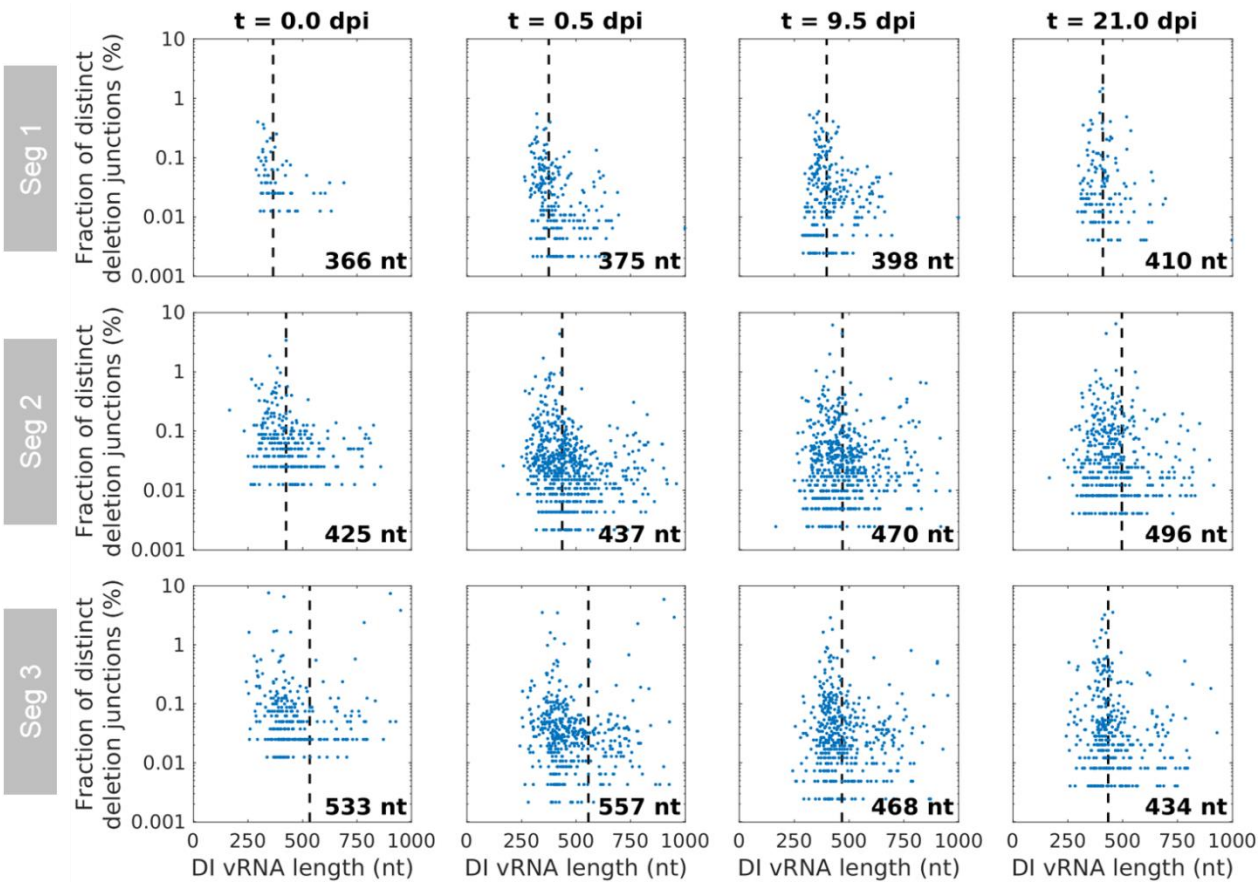

Figure 3: Dependency of the length of DI vRNAs on their accumulation during semi-continuous propagation of IAV. Deletion junctions were identified by Illumina-based NGS and subsequently analyzed via the ViReMa algorithm (Alnaji et al., 2019). Fractions of distinct deletion junctions were calculated based on the ratio of the number of NGS reads of one distinct deletion junction to the number of NGS reads of all deletion junctions of all eight segments. Means of DI vRNA length (calculated by fitting a normal distribution function) are indicated by dashed vertical lines and corresponding lengths are given at the bottom right. Representative time points are illustrated.

3.4 The incorporation signal, but not the entire bundling signal, is required for propagation of DIPs

We next examined the position of the breaking points of DI vRNAs. Fig. 4 illustrates the position of distinct deletion junction, as indicated by the number of retained nucleotides prior (DI vRNA 3´ length, negative-sense, in 3´ to 5´ orientation) and after (DI vRNA 5´ length) the deletion junction site. In the course of the semi-continuous cultivation, breaking points were mostly located in proximity to both ends of vRNA (Fig. 4). This finding is in line with our observation of the

predominant accumulation of short DI vRNAs (Fig. 3.). We also observed highly abundant medium-sized DI vRNAs on Seg 3 in the seed virus (0.0 dpi). Yet, the fraction of DI vRNAs carrying these deletions decreased, or corresponding DI vRNAs even disappeared towards the end of cultivation (Fig. 3). Again, this indicates that shorter DI vRNAs replicate faster and outcompete longer ones. Additionally, the 3´ length of the DI vRNA did largely not correlate with the 5´ length, suggesting that deletion junctions are not preferably symmetrical.

While the lengths of the 3´ and 5´ ends ranged from below 100 nt to over 500 nt, specific minimum lengths were retained in the DI vRNAs (Fig. 4). We then asked whether the complete packaging signal, which is important for organized packaging into progeny virions, was unaffected by deletions. A small percentage of breaking points was located in the packaging signal (on Seg 1 and 2); yet, the majority of the deletion junction sites were located outside of it, which is in line with the observation of a sweet spot in DI vRNA length (Fig. 3). For a more thorough investigation of deletion junctions in the packaging signal, we highlighted the positions of the incorporation signal (NCR) and the bundling signal (terminal ends of coding region) (Goto et al., 2013). We checked which part of the sequence at both ends needs to be retained for a functional replication and packaging of the truncated vRNA, assuming that only propagation-competent DI vRNAs can be detected. No deletion junctions in the incorporation signal for the polymerase segments as well as for Seg 4–8 were identified (Fig. 4, Supplementary Fig. 3, respectively). Therefore, we suggest that the preservation of the entire incorporation signal is crucial for a propagation of DIPs

Interestingly, deletion junctions in the bundling signal (on Seg 1 and 2) could be detected, indicating that the entire bundling signal of these segments is most likely not required for propagation of DIPs. In particular, clusters of DI vRNA breaking points in the bundling signal were stable and present over the complete course of the semi-continuous cultivation. In contrast, Seg 3

did not show any breaking points in both signals. Moreover, we found a minimum sequence length of 84 nt (3´ end) and 100 nt (5´ end), 25 nt and 95 nt, and 82 nt and 95 nt for Seg 1, 2, and 3, respectively. Supplementary Fig. 3 shows the position of deletion junction sites in Seg 4–8. Notably, although only very few distinct deletion junctions were detected, breaking points were found in the bundling signal on Seg 6 (3´ end), 7 (both ends), and 8 (5´ end).

In summary, our results show that the complete incorporation signal is crucial for propagation of DIPs. Yet, only parts of the bundling signal in Seg 1 and 2 seem to be required for DIP spreading.

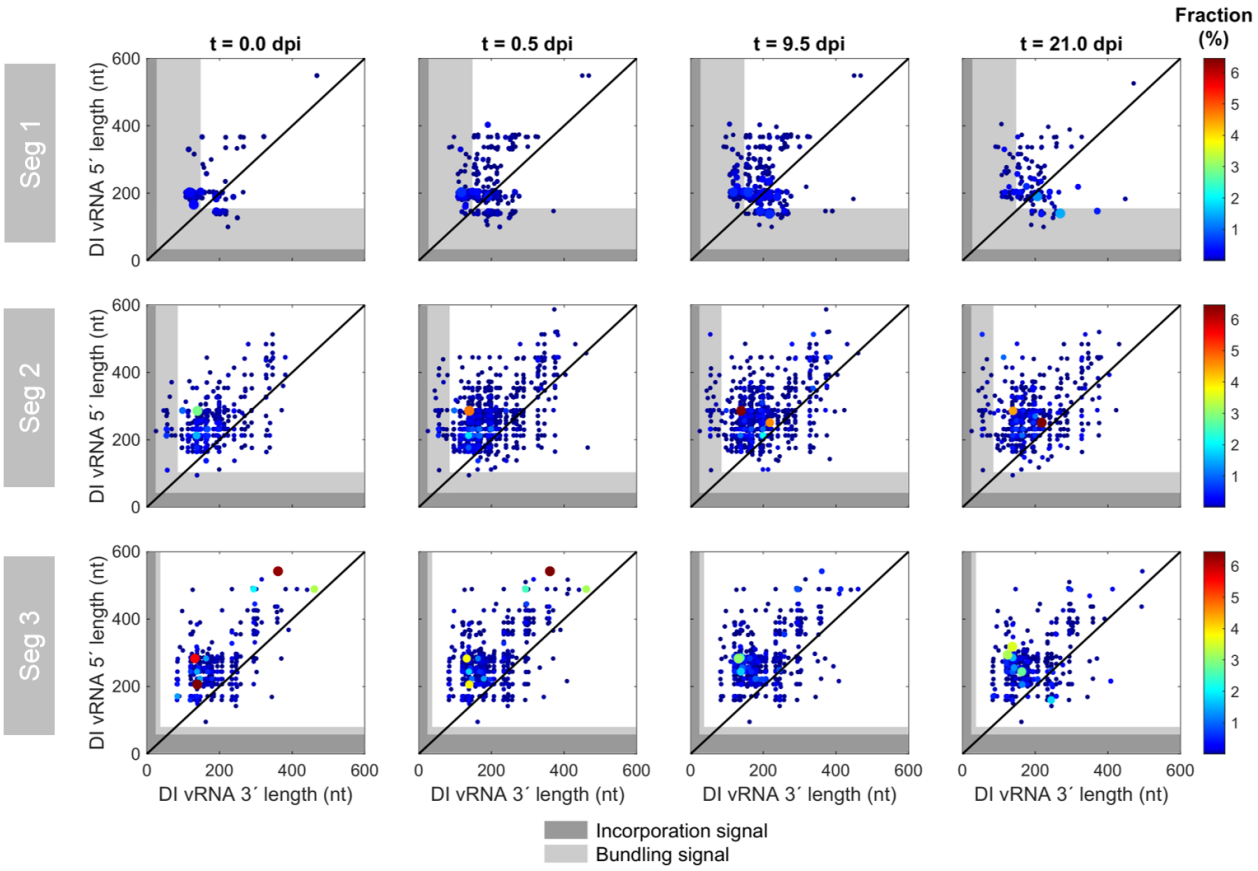

Figure 4: Deletion junction sites of DI vRNAs during semi-continuous propagation of IAV. Deletion junctions were identified by Illumina-based NGS and subsequently analyzed via the ViReMa algorithm (Alnaji et al., 2019). DI vRNA 3´ and 5' length indicates the number of retained nucleotides prior and after the deletion junction at the respective vRNA ends (negative-sense, in 3´ to 5´ orientation). The packaging signal is indicated as grey area, which is divided into the incorporation signal (dark grey area) and bundling signal (light grey area). Representative time

points are illustrated. The color code from red to blue shown on the right denotes the fraction of an individual deletion junction compared to the total number of deletion junctions on all segments. Additionally, the circle radii increase with higher fractions. The diagonal black line indicates an equal DI vRNA 3´ and 5´length.

3.5 Dynamic competition in propagation between DI vRNAs leads to selection of potentially strong candidates for antiviral therapy

In order to elucidate whether the various DI vRNAs show differences in their propagation, we next studied the composition of deletion junctions over cultivation time. More specifically, we determined the fraction of each individual deletion junction over time. Fig. 5A shows these fractions and highlights the top 5 deletion junctions that showed the highest gain or largest loss from the seed virus (0 dpi) to the end of cultivation (21 dpi). Likewise, the top 5 gains of *de novo* formed DI vRNAs are indicated. Note that the latter were not present in the seed virus. Interestingly, differences between gains and losses were very pronounced, with a decreasing fraction of the top 5 losses, while the top 5 gains (including *de novo* DI vRNAs) showed a strong accumulation. These trends were most pronounced for Seg 3. Of note is also one deletion junction on Seg 2 that was present at a very high fraction in the seed virus and throughout the whole cultivation. Furthermore, pronounced shifts in the composition of deletion junctions were found for 9–9.5 and 17–17.5 dpi, at best visible for Seg 3. The occurrence of DI vRNAs that accumulate faster and achieve higher fractions than other DI vRNAs suggests that there was a dynamic competition in the propagation between distinct DI vRNAs. Assuming that fast-propagating DI vRNAs consume more cellular resources and are preferentially packaged (constituting interference), it may have ultimately led to the selection of highly interfering DIPs.

Finally, we examined whether top gains (including *de novo* DI vRNAs) and losses show differences in the deletion junction position (Fig. 5B). To get a better overview, we expanded the number of the top candidates in each category to 15. However, it appeared that no clear differences between

the groups were present. For both gains and losses, few deletion junction sites were located in the bundling signal for Seg 1 and 2 (although most were found outside (Fig. 5B)), but none for Seg 3. For the top 100 candidates, similar results were observed (Supplementary Fig. 4). Therefore, even for competitive DIPs (which require an efficient packaging process), we found a shorter packaging signal compared to the FL vRNA on Seg 1 (both ends) and on Seg 2 (3´ end), which further emphasizes that DIPs do not require the entire bundling signal for fast replication and spread. Please also note a few DI vRNAs (belonging to the top 15 losses) on Seg 3 showing a medium-sized DI vRNA length (~900 nt) (Fig. 5B, upper right corner), which is in line with our observation that long DI vRNAs accumulate to low fractions (Fig. 3). Yet, we also found two top 15 gains (*de novo* DI vRNAs) on Seg 2 with a very long DI vRNA (1905 nt and 1628 nt) (Supplementary Fig. 4A). This finding might suggest that not only the sequence length but also the breaking point position and probably further unknown regulatory effects are crucial for the efficient propagation of DI vRNAs. In addition, our analysis showed a cluster of breaking points in Seg 3 of top 100 gains (*de novo* DI vRNAs) at a DI vRNA 3´ length of approximately 120–180 nt, indicating a preferred spot for deletions (Supplementary Fig. 4B).

In summary, it appears that the semi-continuous production of IAV led to the selection of well propagating DI vRNAs. Moreover, breaking points of competitive DI vRNAs were found within the bundling signal, indicating that their packaging signal is shorter compared to the FL vRNA on Seg 1 (both ends) and Seg 2 (3´ end). In addition, data suggest that not only the length but also the deletion junction position may be a decisive factor for high propagating DI vRNAs. Finally, DI vRNAs showing the highest fraction at the end of cultivation may be strong candidates for antiviral treatment.

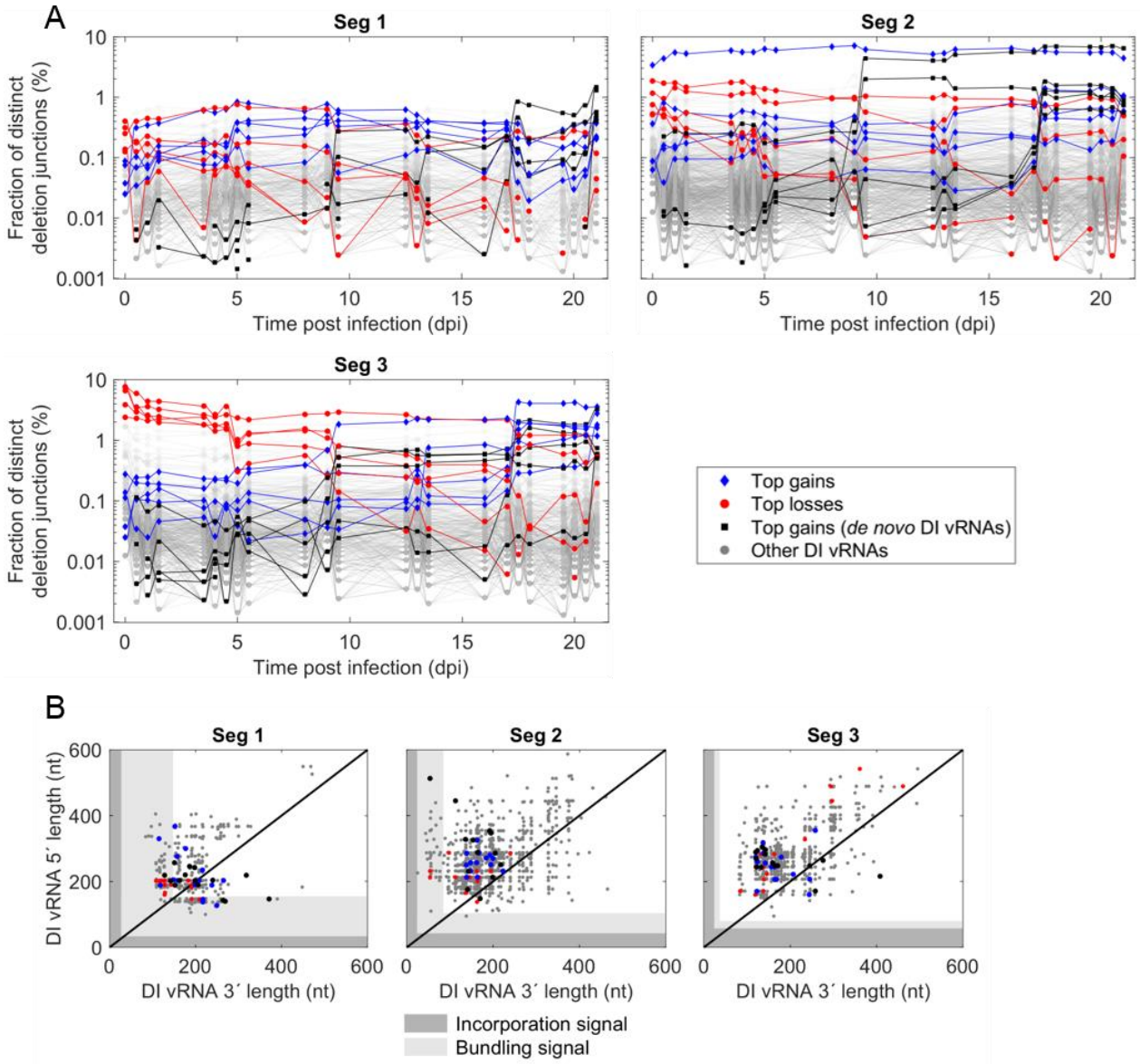

Figure 5: Propagation of DI vRNAs showing highest gains or losses during semi-continuous propagation of IAV. Deletion junctions were identified by Illumina-based NGS and subsequently analyzed via the ViReMa algorithm (Alnaji et al., 2019). Fractions of distinct deletion junctions were calculated based on the ratio of the number of NGS reads of one distinct deletion junction to the number of NGS reads of all deletion junctions of all eight segments. (A) Fraction of distinct DI vRNAs belonging to the group of top 5 gains, losses and gains of *de novo* generated DI vRNAs over cultivation time. Top gains and losses represent deletion junctions showing the highest increase or decrease of their fraction over the cultivation, respectively. Top gains of *de novo* generated DI vRNAs indicate newly formed deletion junctions with the highest fraction at the end of cultivation. (B) Deletion junction position of the top 15 gains, losses and gains of *de novo* formed DI vRNAs. DI vRNA 3´ and 5’ length indicates the number of retained nucleotides prior and subsequent to the deletion junction at the respective vRNA ends (negative-sense, in 3´ to 5´ orientation). The

packaging signal is indicated as grey area, which is divided into the incorporation signal (dark grey area) and bundling signal (light grey area).

4 Discussion

The administration of DIPs has been proposed for antiviral therapy against influenza virus infections. In this study, we investigated the selection of competitive DIPs for identification of strong candidates for antiviral therapy using a semi-continuous cultivation strategy. For this, we quantified distinct deletion junctions using a recently published NGS framework (Alnaji et al., 2019). In principle, DIPs and STVs are in a competition for cellular and viral resources (for instance the viral polymerases) (Marriott and Dimmock, 2010; Widjaja et al., 2012), thus, the replication advantage of DIPs is one mechanism for suppression and interference with STV (Laske et al., 2016; Marriott and Dimmock, 2010; Nayak et al., 1985). Moreover, it was shown that DIPs interfere with STV propagation at the packaging step (Duhaut and McCauley, 1996; Odagiri and Tashiro, 1997). We propose that DI vRNAs showing the highest propagation possess the highest interference capacity with FL vRNA. In addition, due to the periodic oscillations of both the total and infectious virus titers (Fig. 1C), DIPs were challenged by alternating high and low MOI conditions, which likely resulted in different selection pressures.

Our data show that the most competitive DI vRNAs are derived from the polymerase segments. We found the highest variation, predominant accumulation and most *de novo* formation of DI vRNAs on the polymerase segments (Fig. 2A, Fig. 2B, Fig. 2C, respectively). This confirms previous studies, which showed that DI vRNAs are preferentially found on Seg 1, 2, and 3 (Davis and Nayak, 1979; Duhaut and Dimmock, 1998; Jennings et al., 1983; Nayak et al., 1985; Saira et al., 2013). In further agreement with this, a bias towards the emergence of DI vRNAs in the polymerase segments was shown for the production of IAV over 17 d in a two-stage bioreactor

system for a fully continuous cultivation (Frensing et al., 2013). Mathematical modeling of the intracellular replication of STVs and DIPs also suggested that DI vRNAs of IAV polymerase segments are more competitive than other segments (Laske et al., 2016). In particular, they even yielded high progeny numbers in less advantageous infections scenarios, i.e., when STV co-infection was delayed by several hours. Furthermore, clonal DI244, a prototypic and well-characterized DIP with a deletion on Seg 1, showed a pronounced antiviral effect in *in vivo* studies (Dimmock et al., 2012; Dimmock et al., 2008; Easton et al., 2011). In addition, a recent study demonstrated that DI vRNAs carrying an internal deletion in Seg 1, 2 or 3 inhibited STV replication not only *in vitro* but also *in vivo* (Zhao et al., 2018).

Based on our results, short DI vRNAs are highly competitive as they accumulated to higher levels in comparison to longer DI vRNAs (Fig. 3). Yet, also a length sweet spot was observed. In general, it is believed that the shorter length of DI vRNAs in comparison to FL vRNAs leads to a replication advantage and, thus, interference with FL vRNA replication (Laske et al., 2016; Marriott and Dimmock, 2010; Nayak et al., 1985). However, we found the highest abundance of DI vRNAs at a length sweet spot indicating an optimal length for DIP replication and spreading (Fig. 3). This finding is supported by the fact that the highly potent DI244 exhibited a similar DI vRNA length like our calculated length optimum for Seg 1 (366–414 nt, Fig. 3) (Dimmock et al., 2012; Dimmock et al., 2008; Easton et al., 2011). Other studies reported a mean DI vRNA length of 400–500 nt for Seg 1, 2, and 3 (Dimmock and Easton, 2014; Duhaut and Dimmock, 1998). For DIPs originating from clinical isolates, a similar mean DI vRNA length of 377 nt (Seg 1), 390 nt (Seg 2), 490 nt (Seg 3) was found (Saira et al., 2013). Supporting the hypothesis of an optimal length, the continuous production of DI244 (in co-infection with STV) in a two-stage bioreactor system resulted in a preserved length of DI vRNA signals in Seg 1 at approximately 400 bp (analyzed by gel electrophoresis, (Tapia et al., 2019)). Another investigation performed via a dual luciferase

reporter assay also confirmed these findings but additionally suggested that the sequence, more specifically the untranslated region and coding region, may also have an influence on DI vRNA competition (Widjaja et al., 2012). This is consistent with previous work proposing that not only the length, but also the sequence may drive the replication advantage of DI vRNAs (Nayak et al., 1985). Indeed, we found a few larger DI vRNAs up to 1000 nt, which accumulated to high fractions (Fig. 3). In addition, two very long DI vRNAs (1905 nt and 1628 nt) were included in the top 15 gains of the *de novo* formed DI vRNAs (Supplementary Fig. 4A). In further agreement, one study evaluated the interfering efficacy of three clonal DI vRNAs with a relatively similar length in a mice model, which differed significantly from each other (Dimmock et al., 2008). These results support the hypothesis that not only the DI vRNA length, but also the deletion junction site and further unknown regulatory effects are decisive factors for competition of DI vRNAs and, thus, also for interference.

The packaging signal is divided into two parts, the incorporation signal and the bundling signal. The incorporation signal is found in the NCR and was reported to lead the packaging of the vRNA in which the signal is found (Goto et al., 2013). Moreover, it includes the highly essential promotor region. The second part of the packaging signal is the bundling signal, which is located at the terminal ends of the coding region and confers the selective packaging of the eight different segments (Goto et al., 2013). Various publications showed that DIPs with defective polymerase segments mostly retain the NCR and parts of the coding region in the truncated segment (Alnaji et al., 2019; Davis et al., 1980; Davis and Nayak, 1979; Duhaut and Dimmock, 2000; Duhaut and Dimmock, 1998; Jennings et al., 1983; Nayak et al., 1982; Saira et al., 2013). So far, very little data was available about a minimum sequence length for non-polymerase segments (Duhaut and Dimmock, 1998; Duhaut and McCauley, 1996; Jennings et al., 1983). In our analysis, we found

minimum sequence lengths (negative-sense, in 3´ to 5´ orientation), which enabled the spread and accumulation of DI vRNAs, of 84 nt (3´ end) and 100 nt (5´ end), 25 nt and 95 nt, and 82 nt and 95 nt for Seg 1, 2, and 3, respectively. Furthermore, the non-polymerase DI vRNAs measured in our analysis enable a general assessment of their minimum lengths. DI vRNAs shorter than the observed lengths may have led to propagation-incompetent DIPs, which could, thus, not be detected. As expected, our results show that the incorporation signal is crucial for DIP propagation as it was unaffected by deletions (Fig. 4). However, several deletion junction sites for both top gains (highly competitive) and losses were located in the bundling signal on Seg 1 at both ends and on Seg 2 at the 3´ end (Fig. 4 and Fig. 5B). For the non-polymerase segments, we found deletion junction sites in the bundling signal on Seg 6 (3´ end), 7 (both ends), and 8 (5´ end) (Supplementary Fig. 3). Therefore, we suggest that DIPs require only parts of the bundling signal for efficient replication and spreading. This finding has not been highlighted in literature so far and was only possible through the identification and quantification of the large number of distinct deletion junctions using a recently published NGS framework (Alnaji et al., 2019). However, our result is in contrast to a previous study, which reported that a minimum DI vRNA 5´ length of 150 nt is required for DI vRNA stability in serial passaging experiments and to confer interference with FL vRNA (Duhaut and Dimmock, 2000). Highest interference was shown for a 5´ end length of 220 nt in Seg 1 (Duhaut and Dimmock, 2002), which implies that the entire packaging signal of Seg 1 (154 nt at 5´ end) is crucial for maximum interference. In line with this, most deletion junction sites were located outside of the bundling signal in the present study. Previous work showed that DI vRNAs interfere with FL vRNAs in the packaging process, by selectively suppressing the packaging either of the parent segment (Duhaut and McCauley, 1996; Odagiri and Tashiro, 1997) or the FL vRNA of another genome segment (Ueda et al., 1980). Furthermore, differences in the packaging rate were found between distinct DI vRNAs (Duhaut and Dimmock, 2002; Duhaut and

McCauley, 1996). Thus, highly abundant DI vRNAs found in the present study may have an advantage in the entire propagation process over others, including both replication and packaging. However, further in-depth studies are required to better characterize the interference of DI vRNAs at the virus assembly step. Overall, our data suggest that highly competitive DI vRNAs do require the complete incorporation signal but not the entire bundling signal for efficient DIP spreading.

Furthermore, our results suggest that a small subset of distinct DI vRNAs of the polymerase segments outcompeted other candidates (Fig. 5A) and, thus, may show high antiviral activity. In addition, the top 5 gains of *de novo* formed DI vRNAs were not present in the seed virus and had to outcompete already existing DI vRNAs, indicating their high competitiveness. Interestingly, we found two pronounced shifts in the composition of the DI vRNA population for 9–9.5 and 17–17.5 dpi (Fig. 5A) indicating a fast increase of a few highly competitive DI vRNAs. One DI vRNA of Seg 2 was already present in the seed virus and persisted during cultivation at a very high fraction underlining the high competitiveness of this potential candidate for antiviral therapy (Fig. 5A). Overall, we found no clear differences in the deletion junction position between both top gains and losses (Fig. 5B). Moreover, a breaking point cluster of top 100 gains (*de novo* DI vRNAs) between a DI vRNA 3´ length of approximately 120–180 nt was observed for Seg 3 (Supplementary Fig. 4B). This observation indicates that deletions may occur preferentially at specific breaking points. Furthermore, we found no correlation between the 3´ length of the DI vRNA and the 5´ length, which suggests that deletion junctions are not preferably symmetrical (Fig. 4).

Taken together, our data support previous work that DI vRNAs are in a competition for propagation. Distinct DI vRNAs that are characterized by a high propagation rate might have a higher capacity to interfere with STV replication. The highly competitive DI vRNAs of the polymerase segments, comprise an optimal DI vRNA length, conserve the incorporation signal,

but do not require the entire bundling signal. In addition, yet unidentified regulatory functions certainly play an additional role during DI vRNAs propagation, in particular during the replication and packaging. Due to the complex features of highly competitive DIPs, we suppose that the best candidates for antiviral therapy are difficult to be designed *in silico*. Thus, evolution studies are a convenient screening tool. In a follow-up study, DIPs harboring the most competitive DI vRNAs identified in this study will be produced using cell lines stably expressing the missing viral proteins to complement the defect of these DIPs (Bdeir et al., 2019). And, further investigations will be performed to characterize these candidates with respect to their interfering efficacy and options for their use in antiviral therapy (Hein et al., 2020; Kupke et al., 2019).

5 Conflict of Interest

The authors declare no conflict of interest

6 Author Contributions

Conceptualization, L.P., D.R., Y.G., S.Y.K. and U.R.; Methodology, D.R., F.G.A.; Investigation, L.P., D.R., F.G.A.; Writing – Original Draft, L.P. and S.Y.K.; Writing – Review & Editing, L.P., D.R., F.G.A., Y.G., C.B.B., S.Y.K. and U.R.; Funding Acquisition, U.R.

7 Acknowledgments

Special thanks to Claudia Best and Nancy Wynserski for their outstanding technical support. We thank Thomas Bissinger for providing the seed virus and Marc Hein and Tanya Dogra for valuable discussions. The authors appreciate the sequencing work of Alvaro Hernandez, Christy Wright and the staff at the Roy. J. Carver Biotechnology Center, University of Illinois. We thank Shanghai BioEngine Sci-Tech and Prof. Tan from the East China University of Science and Technology for supplying the Xeno™ medium. The work was supported by the Defense Advanced Research

Projects Agency (https://www.darpa.mil/program/intercept), INTERCEPT program under Cooperative Agreement W911NF-17-2-0012.

8 References

Alnaji, F.G., Holmes, J.R., Rendon, G., Vera, J.C., Fields, C.J., Martin, B.E., and Brooke, C.B. (2019). Sequencing Framework for the Sensitive Detection and Precise Mapping of Defective Interfering Particle-Associated Deletions across Influenza A and B Viruses. J Virol *93*. doi:10.1128/JVI.00354-19.

Bdeir, N., Arora, P., Gartner, S., Hoffmann, M., Reichl, U., Pohlmann, S., and Winkler, M. (2019). A system for production of defective interfering particles in the absence of infectious influenza A virus. PLoS One *14*, e0212757. doi:10.1371/journal.pone.0212757.

Bissinger, T., Fritsch, J., Mihut, A., Wu, Y., Liu, X., Genzel, Y., Tan, W.S., and Reichl, U. (2019). Semi-perfusion cultures of suspension MDCK cells enable high cell concentrations and efficient influenza A virus production. Vaccine *37*, 7003-7010. doi:10.1016/j.vaccine.2019.04.054.

Breen, M., Nogales, A., Baker, S.F., and Martinez-Sobrido, L. (2016). Replication-Competent Influenza A Viruses Expressing Reporter Genes. Viruses *8*. doi:10.3390/v8070179.

Davis, A.R., Hiti, A.L., and Nayak, D.P. (1980). Influenza defective interfering viral RNA is formed by internal deletion of genomic RNA. Proceedings of the National Academy of Sciences of the United States of America *77*, 215-219. doi:10.1073/pnas.77.1.215.

Davis, A.R., and Nayak, D.P. (1979). Sequence relationships among defective interfering influenza viral RNAs. Proceedings of the National Academy of Sciences of the United States of America *76*, 3092-3096. doi:10.1073/pnas.76.7.3092.

Dimmock, N.J., Dove, B.K., Meng, B., Scott, P.D., Taylor, I., Cheung, L., Hallis, B., Marriott, A.C., Carroll, M.W., and Easton, A.J. (2012). Comparison of the protection of ferrets against pandemic 2009 influenza A virus (H1N1) by 244 DI influenza virus and oseltamivir. Antiviral Res *96*, 376-385. doi:10.1016/j.antiviral.2012.09.017.

Dimmock, N.J., and Easton, A.J. (2014). Defective interfering influenza virus RNAs: time to reevaluate their clinical potential as broad-spectrum antivirals? J Virol *88*, 5217-5227. doi:10.1128/JVI.03193-13.

Dimmock, N.J., Rainsford, E.W., Scott, P.D., and Marriott, A.C. (2008). Influenza virus protecting RNA: an effective prophylactic and therapeutic antiviral. J Virol *82*, 8570-8578. doi:10.1128/JVI.00743-08.

Duhaut, S., and Dimmock, N.J. (2000). Approximately 150 Nucleotides from the 5′ End of an Influenza A Segment 1 Defective Virion RNA Are Needed for Genome Stability during Passage of Defective Virus in Infected Cells. Virology *275*, 278-285. doi:10.1006/viro.2000.0502.

Duhaut, S.D., and Dimmock, N.J. (1998). Heterologous Protection of Mice from a Lethal Human H1N1 Influenza A Virus Infection by H3N8 Equine Defective Interfering Virus: Comparison of Defective RNA Sequences Isolated from the DI Inoculum and Mouse Lung. Virology *248*, 241-253. doi:10.1006/viro.1998.9267.

Duhaut, S.D., and Dimmock, N.J. (2002). Defective segment 1 RNAs that interfere with production of infectious influenza A virus require at least 150 nucleotides of 5′ sequence: evidence from a plasmid-driven system. Journal of General Virology *83*, 403-411. doi:10.1099/0022-1317-83-2-403.

Duhaut, S.D., and McCauley, J.W. (1996). Defective RNAs inhibit the assembly of influenza virus genome segments in a segment-specific manner. Virology *216*, 326-337. doi:10.1006/viro.1996.0068.

Easton, A.J., Scott, P.D., Edworthy, N.L., Meng, B., Marriott, A.C., and Dimmock, N.J. (2011). A novel broad-spectrum treatment for respiratory virus infections: influenza-based defective interfering virus provides protection against pneumovirus infection in vivo. Vaccine *29*, 2777-2784. doi:10.1016/j.vaccine.2011.01.102.

Frensing, T., Heldt, F.S., Pflugmacher, A., Behrendt, I., Jordan, I., Flockerzi, D., Genzel, Y., and Reichl, U. (2013). Continuous influenza virus production in cell culture shows a periodic accumulation of defective interfering particles. PLoS One *8*, e72288. doi:10.1371/journal.pone.0072288.

Frensing, T., Kupke, S.Y., Bachmann, M., Fritzsche, S., Gallo-Ramirez, L.E., and Reichl, U. (2016). Influenza virus intracellular replication dynamics, release kinetics, and particle morphology during propagation in MDCK cells. Appl Microbiol Biotechnol *100*, 7181-7192. doi:10.1007/s00253-016-7542-4.

Fujii, Y., Goto, H., Watanabe, T., Yoshida, T., and Kawaoka, Y. (2003). Selective incorporation of influenza virus RNA segments into virions. Proceedings of the National Academy of Sciences *100*, 2002-2007. doi:10.1073/pnas.0437772100.

Genzel, Y., and Reichl, U. (2007). Vaccine Production. In Animal Cell Biotechnology: Methods and Protocols, R. Pörtner, ed. (Totowa, NJ: Humana Press), pp. 457-473.

Goto, H., Muramoto, Y., Noda, T., and Kawaoka, Y. (2013). The genome-packaging signal of the influenza A virus genome comprises a genome incorporation signal and a genome-bundling signal. J Virol *87*, 11316-11322. doi:10.1128/JVI.01301-13.

Hayden, F.G., Sugaya, N., Hirotsu, N., Lee, N., de Jong, M.D., Hurt, A.C., Ishida, T., Sekino, H., Yamada, K., Portsmouth, S., *et al.* (2018). Baloxavir Marboxil for Uncomplicated Influenza in Adults and Adolescents. N Engl J Med *379*, 913-923. doi:10.1056/NEJMoa1716197.

Hein, M.D., Kollmus, H., Marichal-Gallardo, P., Puttker, S., Benndorf, D., Genzel, Y., Schughart, K., Kupke, S.Y., and Reichl, U. (2020). OP7, a novel influenza A virus defective interfering particle: production, purification, and animal experiments demonstrating antiviral potential. Appl Microbiol Biotechnol. doi:10.1007/s00253-020-11029-5.

Huo, C., Cheng, J., Xiao, J., Chen, M., Zou, S., Tian, H., Wang, M., Sun, L., Hao, Z., and Hu, Y. (2020). Defective Viral Particles Produced in Mast Cells Can Effectively Fight Against Lethal Influenza A Virus. Front Microbiol *11*, 553274. doi:10.3389/fmicb.2020.553274.

Hurt, A.C., Ernest, J., Deng, Y.M., Iannello, P., Besselaar, T.G., Birch, C., Buchy, P., Chittaganpitch, M., Chiu, S.C., Dwyer, D., *et al.* (2009). Emergence and spread of oseltamivir-resistant A(H1N1) influenza viruses in Oceania, South East Asia and South Africa. Antiviral Res *83*, 90-93. doi:10.1016/j.antiviral.2009.03.003.

Hutchinson, E.C., von Kirchbach, J.C., Gog, J.R., and Digard, P. (2010). Genome packaging in influenza A virus. J Gen Virol *91*, 313-328. doi:10.1099/vir.0.017608-0.

Jennings, P.A., Finch, J.T., Winter, G., and Robertson, J.S. (1983). Does the higher order structure of the influenza virus ribonucleoprotein guide sequence rearrangements in influenza viral RNA? Cell *34*, 619-627. doi:10.1016/0092-8674(83)90394-X.

Jones, J.C., Kumar, G., Barman, S., Najera, I., White, S.W., Webby, R.J., and Govorkova, E.A. (2018). Identification of the I38T PA Substitution as a Resistance Marker for Next-Generation Influenza Virus Endonuclease Inhibitors. mBio *9*. doi:10.1128/mBio.00430-18.

Kawakami, E., Watanabe, T., Fujii, K., Goto, H., Watanabe, S., Noda, T., and Kawaoka, Y. (2011). Strand-specific real-time RT-PCR for distinguishing influenza vRNA, cRNA, and mRNA. J Virol Methods *173*, 1-6. doi:10.1016/j.jviromet.2010.12.014.

Kupke, S.Y., Riedel, D., Frensing, T., Zmora, P., and Reichl, U. (2019). A Novel Type of Influenza A Virus-Derived Defective Interfering Particle with Nucleotide Substitutions in Its Genome. Journal of Virology *93*, e01786-01718. doi:10.1128/jvi.01786-18.

Laske, T., Heldt, F.S., Hoffmann, H., Frensing, T., and Reichl, U. (2016). Modeling the intracellular replication of influenza A virus in the presence of defective interfering RNAs. Virus Res *213*, 90-99. doi:10.1016/j.virusres.2015.11.016.

Lohr, V., Genzel, Y., Behrendt, I., Scharfenberg, K., and Reichl, U. (2010). A new MDCK suspension line cultivated in a fully defined medium in stirred-tank and wave bioreactor. Vaccine *28*, 6256-6264. doi:10.1016/j.vaccine.2010.07.004.

Marriott, A.C., and Dimmock, N.J. (2010). Defective interfering viruses and their potential as antiviral agents. Rev Med Virol *20*, 51-62. doi:10.1002/rmv.641.

Moa, A.M., Chughtai, A.A., Muscatello, D.J., Turner, R.M., and MacIntyre, C.R. (2016). Immunogenicity and safety of inactivated quadrivalent influenza vaccine in adults: A systematic review and meta-analysis of randomised controlled trials. Vaccine *34*, 4092-4102. doi:10.1016/j.vaccine.2016.06.064.

Nayak, D.P., Chambers, T.M., and Akkina, R.K. (1985). Defective-Interfering (DI) RNAs of Influenza Viruses: Origin, Structure, Expression, and Interference. In Current Topics in Microbiology and Immunology, M. Cooper, H. Eisen, W. Goebel, P.H. Hofschneider, H. Koprowski, F. Melchers, M. Oldstone, R. Rott, H.G. Schweiger, P.K. Vogt, *et al.*, eds. (Berlin, Heidelberg: Springer Berlin Heidelberg), pp. 103-151.

Nayak, D.P., Sivasubramanian, N., Davis, A.R., Cortini, R., and Sung, J. (1982). Complete sequence analyses show that two defective interfering influenza viral RNAs contain a single internal deletion of a polymerase gene. Proceedings of the National Academy of Sciences *79*, 2216-2220. doi:10.1073/pnas.79.7.2216.

Noda, T., and Kawaoka, Y. (2010). Structure of influenza virus ribonucleoprotein complexes and their packaging into virions. Rev Med Virol *20*, 380-391. doi:10.1002/rmv.666.

O'Hanlon, R., and Shaw, M.L. (2019). Baloxavir marboxil: the new influenza drug on the market. Current Opinion in Virology *35*, 14-18. doi:10.1016/j.coviro.2019.01.006.

Odagiri, T., and Tashiro, M. (1997). Segment-specific noncoding sequences of the influenza virus genome RNA are involved in the specific competition between defective interfering RNA and its

progenitor RNA segment at the virion assembly step. Journal of virology *71*, 2138-2145. doi:10.1128/JVI.71.3.2138-2145.1997.

Paget, J., Spreeuwenberg, P., Charu, V., Taylor, R.J., Iuliano, A.D., Bresee, J., Simonsen, L., Viboud, C., Global Seasonal Influenza-associated Mortality Collaborator, N., and Teams*, G.L.C. (2019). Global mortality associated with seasonal influenza epidemics: New burden estimates and predictors from the GLaMOR Project. J Glob Health *9*, 020421. doi:10.7189/jogh.09.020421.

Paules, C., and Subbarao, K. (2017). Influenza. The Lancet *390*, 697-708. doi:10.1016/s0140-6736(17)30129-0.

Routh, A., and Johnson, J.E. (2014). Discovery of functional genomic motifs in viruses with ViReMa-a Virus Recombination Mapper-for analysis of next-generation sequencing data. Nucleic Acids Res *42*, e11. doi:10.1093/nar/gkt916.

Saira, K., Lin, X., DePasse, J.V., Halpin, R., Twaddle, A., Stockwell, T., Angus, B., Cozzi-Lepri, A., Delfino, M., Dugan, V., *et al.* (2013). Sequence analysis of in vivo defective interfering-like RNA of influenza A H1N1 pandemic virus. J Virol *87*, 8064-8074. doi:10.1128/JVI.00240-13.

Samson, S.I., Leventhal, P.S., Salamand, C., Meng, Y., Seet, B.T., Landolfi, V., Greenberg, D., and Hollingsworth, R. (2019). Immunogenicity of high-dose trivalent inactivated influenza vaccine: a systematic review and meta-analysis. Expert Rev Vaccines *18*, 295-308. doi:10.1080/14760584.2019.1575734.

Tapia, F., Jordan, I., Genzel, Y., and Reichl, U. (2017). Efficient and stable production of Modified Vaccinia Ankara virus in two-stage semi-continuous and in continuous stirred tank cultivation systems. PLoS One *12*, e0182553. doi:10.1371/journal.pone.0182553.

Tapia, F., Laske, T., Wasik, M.A., Rammhold, M., Genzel, Y., and Reichl, U. (2019). Production of Defective Interfering Particles of Influenza A Virus in Parallel Continuous Cultures at Two Residence Times—Insights From qPCR Measurements and Viral Dynamics Modeling. Frontiers in Bioengineering and Biotechnology *7*. doi:10.3389/fbioe.2019.00275.

Tricco, A.C., Chit, A., Soobiah, C., Hallett, D., Meier, G., Chen, M.H., Tashkandi, M., Bauch, C.T., and Loeb, M. (2013). Comparing influenza vaccine efficacy against mismatched and matched strains: a systematic review and meta-analysis. BMC Medicine *11*, 153. doi:10.1186/1741-7015-11-153.

Ueda, M., Nakajima, K., and Sugiura, A. (1980). Extra RNAs of von Magnus particles of influenza virus cause reduction of particular polymerase genes. Journal of virology *34*, 1-8. doi:10.1128/JVI.34.1.1-8.1980.

Vignuzzi, M., and Lopez, C.B. (2019). Defective viral genomes are key drivers of the virus-host interaction. Nat Microbiol *4*, 1075-1087. doi:10.1038/s41564-019-0465-y.

Vogel, O.A., and Manicassamy, B. (2020). Broadly Protective Strategies Against Influenza Viruses: Universal Vaccines and Therapeutics. Frontiers in Microbiology *11*. doi:10.3389/fmicb.2020.00135.

Widjaja, I., de Vries, E., Rottier, P.J., and de Haan, C.A. (2012). Competition between influenza A virus genome segments. PLoS One *7*, e47529. doi:10.1371/journal.pone.0047529.

Yang, Y., Lyu, T., Zhou, R., He, X., Ye, K., Xie, Q., Zhu, L., Chen, T., Shen, C., Wu, Q., *et al.* (2019). The Antiviral and Antitumor Effects of Defective Interfering Particles/Genomes and Their Mechanisms. Frontiers in Microbiology *10*. doi:10.3389/fmicb.2019.01852.

Zhao, H., To, K.K.W., Chu, H., Ding, Q., Zhao, X., Li, C., Shuai, H., Yuan, S., Zhou, J., Kok, K.H., *et al.* (2018). Dual-functional peptide with defective interfering genes effectively protects mice against avian and seasonal influenza. Nat Commun *9*, 2358. doi:10.1038/s41467-018-04792-7.